Title

Orbital Delocalization and Enhancement of Magnetic Interactions in Perovskite Oxyhydrides

Journal

Scientific Reports, 6(1)

ISSN

2045-2322

Authors

Liu, Kai
Hou, Yusheng
Gong, Xingao
et al.

Publication Date

2016

DOI

10.1038/srep19653

Peer reviewed

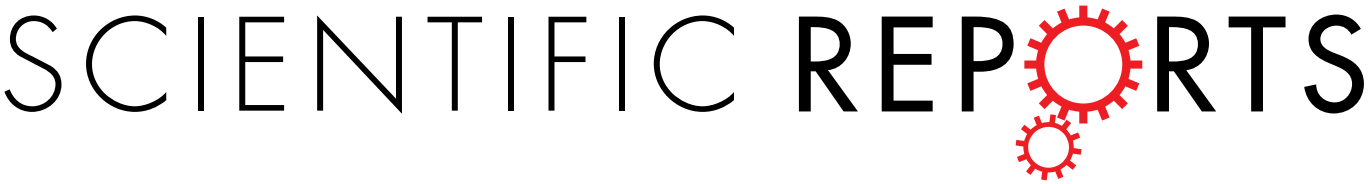

OPEN

Orbital Delocalization and Enhancement of Magnetic Interactions in Perovskite Oxyhydrides

Received: 15 September 2015
Accepted: 16 November 2015
Published: 25 January 2016

Kai Liu, Yusheng Hou, Xingao Gong & Hongjun Xiang

Recent experiments showed that some perovskite oxyhydrides have surprisingly high magnetic-transition temperature. In order to unveil the origin of this interesting phenomenon, we investigate the magnetism in $SrCrO_2H$ and $SrVO_2H$ on the basis of first-principles calculations and Monte Carlo simulations. Our work indicates that the Cr-O-Cr superexchange interaction in $SrCrO_2H$ is unexpectedly strong. Different from the previous explanation in terms of the H^- ion substitution induced increase of the Cr-O-Cr bond angle, we reveal instead that this is mainly because the 3*d* orbitals in perovskite oxyhydrides becomes more delocalized since H^- ions have weaker electronegativity and less electrons than O^{2-} ions. The delocalized 3*d* orbitals result in stronger Cr-O interactions and enhance the magnetic-transition temperature. This novel mechanism is also applicable to the case of $SrVO_2H$. Furthermore, we predict that $SrFeO_2H$ will have unprecedented high Neel temperature because of the extraordinarily strong Fe-H-Fe σ-type interactions. Our work suggests the anion substitution can be used to effectively manipulate the magnetic properties of perovskite compounds.

Complex transition metal oxides have been the subject of enduring interest due to the wide variety of physical properties they exhibit, to name a few, high-T_c superconductivity, magnetoresistance, multiferroicity, thermoelectric response, and so on[1–7]. For the past few years, scientists have found that replacing segmental O^{2-} ions in transition metal oxides by N^{3-}, F^- or S^{2-} can result in novel materials such as pigments, water-splitting photocatalysis, dielectric and cathode material[8–12]. Different from N^{3-}, F^- or S^{2-} which has *p* valence electrons, the H^- anion has a filled $1s^2$ electronic configuration that is fundamentally different from the O^{2-} ion case. Therefore, it is expected that the H^- ion substitution might leads to exotic behaviors in perovskite. In pioneering works, a large amount of hydrogen species were incorporated into $ATiO_3$ (A = Ba, Sr, Ca) and Sr_2VO_4 lattice through the use of CaH_2 reductant[13–16]. The resulting oxyhydride $ATiO_{3-x}H_x$ exhibits high electronic conductivity and its hydride ions are exchangeable with gaseous hydrogen at elevated temperature, indicating that it can be an ideal mixed electron/hydride proton conductor for electrochemical applications[13–15]. In oxyhydride $Sr_2VO_{4-x}H_x$, the hydride ion could act as an effective carrier dopant because the hydrogen and oxygen concentrations can be controlled[16].

Interestingly, it was experimentally found that the magnetic properties of transition metal oxides may change dramatically if some oxygen anions are replaced by hydrogen anions. An antiferromagnetic-to-ferromagnetic transition in $EuTiO_{3-x}H_x$ induced by hydride substitution was reported, where the ferromagnetism was caused by the Ruderman–Kittel–Kasuya–Yosida (RKKY) interaction between the Eu^{2+} spins mediated by the itinerant Ti 3*d* electrons[17]. $LaSrCoO_3H_{0.7}$[18–20] and $Sr_3Co_2O_{4.33}H_{0.84}$[21] were found to display high magnetic transition temperatures. Recently, the stoichiometric perovskite oxyhydrides $SrCrO_2H$ and $SrVO_2H$ have been synthesized[22,23]. The average structure of $SrCrO_2H$ is the cubic perovskite where the hydride ions are randomly distributed. In $SrVO_2H$, the planar VO_2 layers are connected by hydride ions. The experimentally observed antiferromagnetic (AFM) Neel temperature (T_N) of $SrCrO_2H$ and $SrVO_2H$ are around 380 K and higher than 300 K[22,23], respectively. It is puzzling that the Neel temperature T_N of $SrCrO_2H$ is higher than that (290 K)[24,25] of $LaCrO_3$. In both $SrCrO_2H$ and $LaCrO_3$, the valence of Cr element is 3+ with the three 3*d* electrons occupying the t_{2g} orbitals, that

Key Laboratory of Computational Physical Sciences (Ministry of Education), State Key Laboratory of Surface Physics, Collaborative Innovation Center of Advanced Microstructures, and Department of Physics, Fudan University, Shanghai 200433, P.R. China. Correspondence and requests for materials should be addressed to H.X. (email: hxiang@fudan.edu.cn)

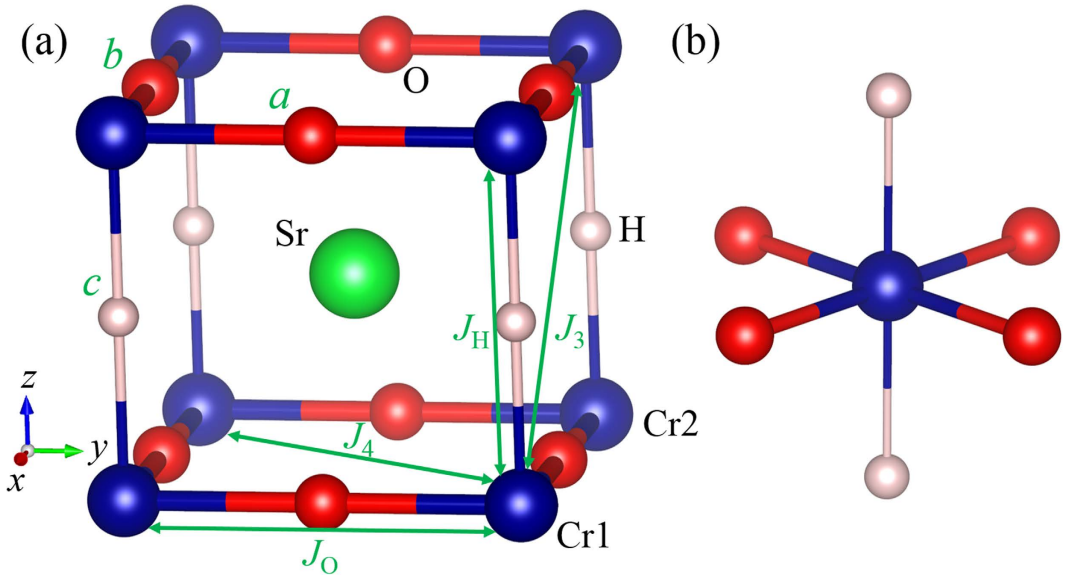

Figure 1. (**a**) Perspective view of the ground state structure of $SrCrO_2H$. The green, blue, red, and greyish spheres represent the Sr^{2+}, Cr^{3+}, O^{2-}, and H^- ions, respectively. The spin exchange paths J_O, J_H, J_3, and J_4 are also indicated. (**b**) The local structure of the CrO_4H_2 octahedron.

is, the electron configuration is $(d_{xy})^1(d_{yz})^1(d_{xz})^1$. In average, each Cr^{3+} ion in $SrCrO_2H$ has two Cr-H-Cr superexchange paths and four Cr-O-Cr superexchange paths. Since the t_{2g} orbitals of the Cr^{3+} ion could not interact with the 1s orbitals of H^- ions by symmetry, the Cr-H-Cr superexchange interaction is negligible. In $LaCrO_3$, there are six Cr-O-Cr superexchange paths for each Cr^{3+} ion. So the fact that the Neel temperature T_N of $SrCrO_2H$ is higher than that of $LaCrO_3$ is rather unexpected.

To probe the origin of the high T_N in $SrCrO_2H$ and $SrVO_2H$, we studied the magnetic properties of $SrCrO_2H$, $SrVO_2H$, and $LaCrO_3$ based on the density functional theory (DFT). We show that due to weaker electronegativity and less electrons of H^- ions than those of O^{2-} ions, the substitution of H^- ions with O^{2-} ions lead to more delocalized 3*d* orbitals of Cr^{3+} ions which make Cr-O-Cr superexchange in $SrCrO_2H$ much stronger and leads to a high T_N. This new mechanism is also applicable to the case of $SrVO_2H$.

Although the H^- ion was experimentally reported to be randomly distributed in $SrCrO_2H$, we will adopt an ordered structure (see Fig. 1a) to investigate the magnetism in $SrCrO_2H$ for the following reasons. First, by using the cluster expansion approach, we find the ground state structure of $SrCrO_2H$ is similar to the experimentally observed structure of $SrVO_2H$. Second, we find that the magnetic properties of another $SrCrO_2H$ structure with a more random H^- ion distribution are similar to those of the ordered structure (see Supplementary Material). The ground state structure (tetragonal *P4/mmm* symmetry) of $SrCrO_2H$ has one H^- ion and two O^{2-} ions in the primitive cell. The Cr^{3+} cations are located within square planes of oxide ions and form CrO_2 sheets. The CrO_2 sheets are connected by hydride ions, which occupy the remaining two coordination sites around each Cr^{3+} center. Thus the ground state structure of $SrCrO_2H$ can be described by a CrO_2-SrH-CrO_2-SrH stacking sequence. The computed phonon frequencies[26] (see Supplementary Figure S3) indicate that the ground state structure of $SrCrO_2H$ is dynamically stable.

To examine the magnetic properties of $SrCrO_2H$, we considered four ordered spin states, namely, the ferromagnetic (FM), A-type AFM, C-type AFM and G-type AFM states. The experimentally observed AFM structure is the G-type. Our GGA + *U* calculations show that all the AFM states have lower energy than the FM state, and the G-type AFM is indeed the ground state, in consistent with experimental observations[22]. To extract the values of the spin exchange parameters, we adopt the four-state mapping approach[27,28]. There are four relevant Cr-Cr spin exchange interactions (see Fig. 1a): (1) J_O is the nearest neighbor (NN) superexchange interaction for the Cr-O-Cr path; (2) J_H is the NN spin exchange interaction for the Cr-H-Cr path; (3) J_3 is next nearest neighbor (NNN) super-superexchange interaction in the plane; (4) J_4 is the NNN out of plane super-superexchange interaction. The calculated exchange parameters in the tetragonal structure of $SrCrO_2H$ are summarized in Table 1. As expected, the NN Cr-O-Cr path has the strongest spin exchange interaction (J_O) since it is mediated by the strong π-π hybridization between 3*d* and 2*p* orbitals. The NN spin exchange interaction J_H is weakly AFM due to the direct through-space overlap between the t_{2g} orbitals of Cr^{3+} ions. The NNN exchange interactions (J_3 and J_4) are negligible. The AFM nature of the NN interactions can result in the G-type AFM order. Based on the calculated spin exchange parameters, our Monte Carlo (MC) simulations indicate that the T_N is around 285 K. If a smaller Hubbard U is adopted, we can get higher T_N according to the theory of superexchange, in better agreement with the experimentally observed T_N[22].

For comparison, we also studied the magnetism in $LaCrO_3$. Experiments show the ground state structure of $LaCrO_3$ is the $GdFeO_3$–type distorted perovskite with *Pbnm* space group and its lattice constants are $a = 5.478$, $b = 7.759$, and $c = 5.516$[29]. The lattice constants of our optimized *Pbnm* structure are $a = 5.468$ Å, $b = 7.758$ Å,

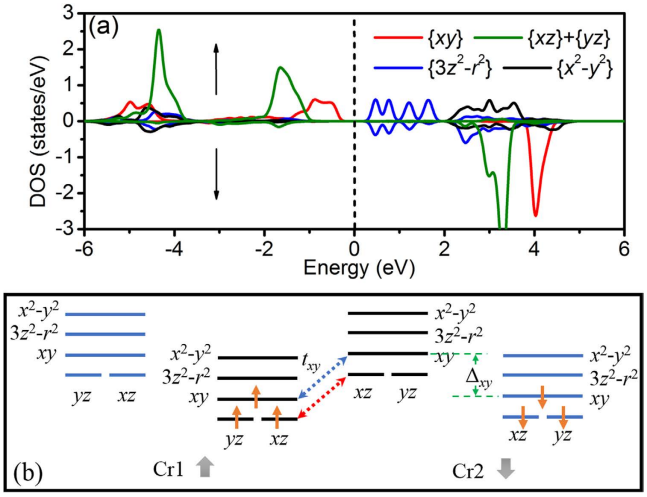

Figure 2. (**a**) PDOS of the spin-up Cr^{3+} ion in $SrCrO_2H$ with the G-type AFM order. (**b**) Energy level and electron occupation for the spin-up Cr1 ion and spin-down Cr2 ion. The positions of Cr1 and Cr2 are shown in Fig. 1a. The spin-up and spin-down levels are denoted by black and blue colors, respectively. The effective orbitals hoppings responsible for the Cr1-Cr2 superexchange interaction are illustrated.

	J_O (meV)	J_H (meV)	J_3 (meV)	J_4 (meV)	T_N (K)
$SrCrO_2H$ (opt.)	23.95	3.26	−0.96	0.34	285
$SrCrO_2H$ (cubic)	29.69	1.27	−1.26	0.69	325
$LaCrO_3$ (opt.)	8.88	–	–	0.38	137
$LaCrO_3$ (cubic)	14.25	–	–	0.73	204
$SrVO_2H$ (opt.)	23.54	1.88	−0.71	0.17	255
$SrFeO_2H$ (opt.)	39.63	89.26	−4.42	4.22	950
$SrFeO_2H$ (cubic)	42.89	70.41	−3.89	−0.91	922

Table 1. Spin exchange parameters and Neel temperature of perovskite systems considered in this work. In $SrCrO_2H$, $SrVO_2H$, and $SrFeO_2H$, the spin exchange paths J_O, J_H, J_3, and J_4 are defined in Fig. 1a. Positive (negative) values indicate that the spin exchange interactions are AFM (FM). The exchange parameters are effective by setting the spin magnitude to 1. In $LaCrO_3$, J_O is the average NN spin exchange parameter and J_4 is the average NNN spin exchange parameter. "opt." refers to the structure optimized by GGA + U calculations, while "cubic" refers to the cubic perovskite structure.

and $c = 5.497$ Å, in good agreement with experiment. The obtained spin exchange parameters of the optimized $LaCrO_3$ are summarized in Table 1. The NN interaction J_O is AFM and the NNN interactions are negligible. This is in accord with the experimentally observed G-type AFM ground state in $LaCrO_3$. Compared with $SrCrO_2H$, it is clear that J_O in $LaCrO_3$ is much weaker. Based on the calculated spin exchange parameters, our MC simulations indicate that the T_N for $LaCrO_3$ is around 133 K. Therefore, our theoretical calculations confirm the experimental observation that $SrCrO_2H$ has a higher T_N than $LaCrO_3$, as shown in Fig. 3.

Now we begin to understand the difference in the magnetic properties between $SrCrO_2H$ and $LaCrO_3$. There are two significant differences between $SrCrO_2H$ and $LaCrO_3$. First, there is a structural difference. The CrO_6 octahedron in $LaCrO_3$ is tilted due to a small tolerance factor, while there is no octahedron tilt in $SrCrO_2H$. As a result, the Cr-O-Cr angle in $SrCrO_2H$ is 180° while the average Cr-O-Cr angle in $LaCrO_3$ is 167°. Second, a chemical difference exists since one third of the O^{2-} ions are replaced by H^- ions.

To make clear whether the structural difference or the chemical difference is responsible for the stronger Cr-O-Cr exchange in $SrCrO_2H$, we investigate the magnetic properties of $SrCrO_2H$ and $LaCrO_3$ with the same cubic perovskite crystal structure. The lattice constant is set to be the average lattice constant (3.85 Å) of experimental $SrCrO_2H$ structure[22]. Note that the hypothetic cubic $LaCrO_3$ phase can be regarded as a result of substituting Sr^{2+} and H^- in cubic $SrCrO_2H$ with La^{3+} and O^{2-}, respectively. The computed spin exchange parameters of these two cubic structures are summarized in Table 1. Surprisingly and interestingly, the Cr-O-Cr superexchange (29.69 meV) in $SrCrO_2H$ is almost as twice as that (14.25 meV) in $LaCrO_3$ despite of the fact that the Cr-O bond length and the Cr-O-Cr bond angle are identical in cubic $SrCrO_2H$ and $LaCrO_3$. As expected, the Cr-O-Cr exchange in cubic $LaCrO_3$ is stronger than that (8.88 meV) in *Pbnm* $LaCrO_3$ according to the Goodenough-Kanamori rule[30–32]. Previously, it was suggested that the structural difference is solely responsible for the high T_N in $SrCrO_2H$[22]. However, our calculations show that the structure difference and chemical difference enhance the Cr-O-Cr exchange interaction by 5.37 meV and 15.44 meV, respectively. Therefore, the effect

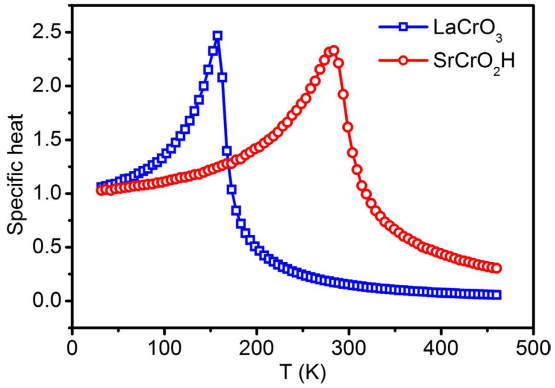

Figure 3. Specific heat of $SrCrO_2H$ and $LaCrO_3$ calculated as a function of temperature from the MC simulations of the classical spin Hamiltonian.

	t_{xz} (eV)	t_{yz} (eV)	t_{xy} (eV)
$SrCrO_2H$ (cubic)	−0.385	0.002	−0.213
$LaCrO_3$ (cubic)	−0.217	−0.017	−0.217

Table 2. Effective hopping between the d_{xz}, d_{yz}, d_{xy} orbitals of nearest neighboring Cr ions in cubic $SrCrO_2H$ and $LaCrO_3$ through the MLWF technique.

of chemical difference on the Cr-Cr exchange interaction is much more important than that of the structural difference.

To account for why J_O in the cubic $SrCrO_2H$ is as twice as that in the cubic $LaCrO_3$, we examine their electronic structures in details. Figure 2a shows the partial density of states (PDOS) of the spin-up Cr^{3+} ion in $SrCrO_2H$ with the G-type AFM order. We can see that, for $SrCrO_2H$, the majority-spin t_{2g} (d_{xy}, d_{xz}, and d_{yz}) orbitals are occupied by three electrons but the majority-spin e_g orbitals are unoccupied, which is similar to the orbital occupation in $LaCrO_3$. The energy level and occupancy of the 3*d* orbitals of the tetragonal $SrCrO_2H$ are shown in Fig. 2b. Note that the t_{2g} orbitals split into the low-lying two-fold degenerate d_{xz}/d_{yz} level and a higher d_{xy} level as a result of the tetragonal symmetry.

Without loss of generality, we consider the spin exchange J_O for the Cr1-O-Cr2 path along the *x* axis, as shown in Fig. 1a. According to Anderson's superexchange theory[33], the magnitude of the spin exchange can be estimated by t^2/Δ, where t is the effective hopping between the d orbitals and Δ is the energy difference between majority-spin and minority-spin orbitals. In the cubic $SrCrO_2H$ or $LaCrO_3$, the d_{xz} orbital can only interact with the neighboring d_{xz} orbital, and so do d_{xy}, d_{yz}. The magnitude of J_O for the Cr1-O-Cr2 path can be estimated as $J_O \propto t_{xz}^2/\Delta_{xz} + t_{yz}^2/\Delta_{yz} + t_{xy}^2/\Delta_{xy}$, where t_m (m=*xz*, *yz*, *xy*) is effective hopping between the m orbitals of Cr1 and Cr2, and Δ_m is the energy difference between the majority-spin *m* orbital and minority-spin *m* orbital of the Cr^{3+} ion (see Fig. 2b). The Δ_m parameters are estimated by constructing the maximally localized Wannier functions (MLWFs) based on the ferromagnetic electronic structure. It turns out that Δ_m (about 5.3 eV) in $SrCrO_2H$ is rather close to that (about 5.5 eV) in $LaCrO_3$. Therefore, we can regard Δ_m as a constant. The effective hopping paramters t_m between the Cr 3*d* orbitals is obtained by constructing the MLWFs using the spin-unpolarized Bloch wavefunctions. These hopping parameters are listed in Table 2. We can see that the hopping parameter t_{yz} between the d_{yz} orbitals of Cr1 and Cr2 is negligible since these two orbitals are almost parallel to each other. The π-π hopping parameter t_{xy} in the cubic $SrCrO_2H$ are the same as that in the cubic $LaCrO_3$. The striking result is that the π-π hopping parameter t_{xz} between the d_{xz} orbitals of Cr1 and Cr2 in the cubic $SrCrO_2H$ is almost 50% stronger than that in $LaCrO_3$. Using these hopping parameters, we can estimate the ratio between J_O in cubic $SrCrO_2H$ and that in $LaCrO_3$ as:

$$\frac{J_O(SrCrO_2H)}{J_O(LaCrO_3)} = \frac{t_{xz}^2(SrCrO_2H) + t_{xy}^2(SrCrO_2H)}{t_{xz}^2(LaCrO_3) + t_{xy}^2(LaCrO_3)} = 2.1.$$

Thus, our first-principles result can be well accounted for by this simple model. This analysis clearly shows that the stronger t_{xz} hopping in $SrCrO_2H$ is responsible for its high T_N.

Figure 4a,b shows the real-space distribution of the d_{xz}-like MLWFs in the cubic $SrCrO_2H$ and $LaCrO_3$. It is clear that the effective d_{xz}-like MLWF not only distributes around the Cr ion, but also has tails on the neighboring O^{2-} ions due to the anti-bonding π^* hybridization between Cr-d_{xz} and O-2*p* orbitals. It is the tails on the O^{2-} ions that mediate the effective hopping between the Cr-d_{xz} orbitals. An interesting observation is that the lobes on the O^{2-} ion in the MLWF of $SrCrO_2H$ are bigger than those in $LaCrO_3$. This suggests that the interaction between Cr-d_{xz} orbital and O-p_z orbital in $SrCrO_2H$ is stronger than that in $LaCrO_3$, in agreement with our previous result that the effective hopping between the d_{xz} orbitals of Cr1 and Cr2 in $SrCrO_2H$ is larger than that in $LaCrO_3$.

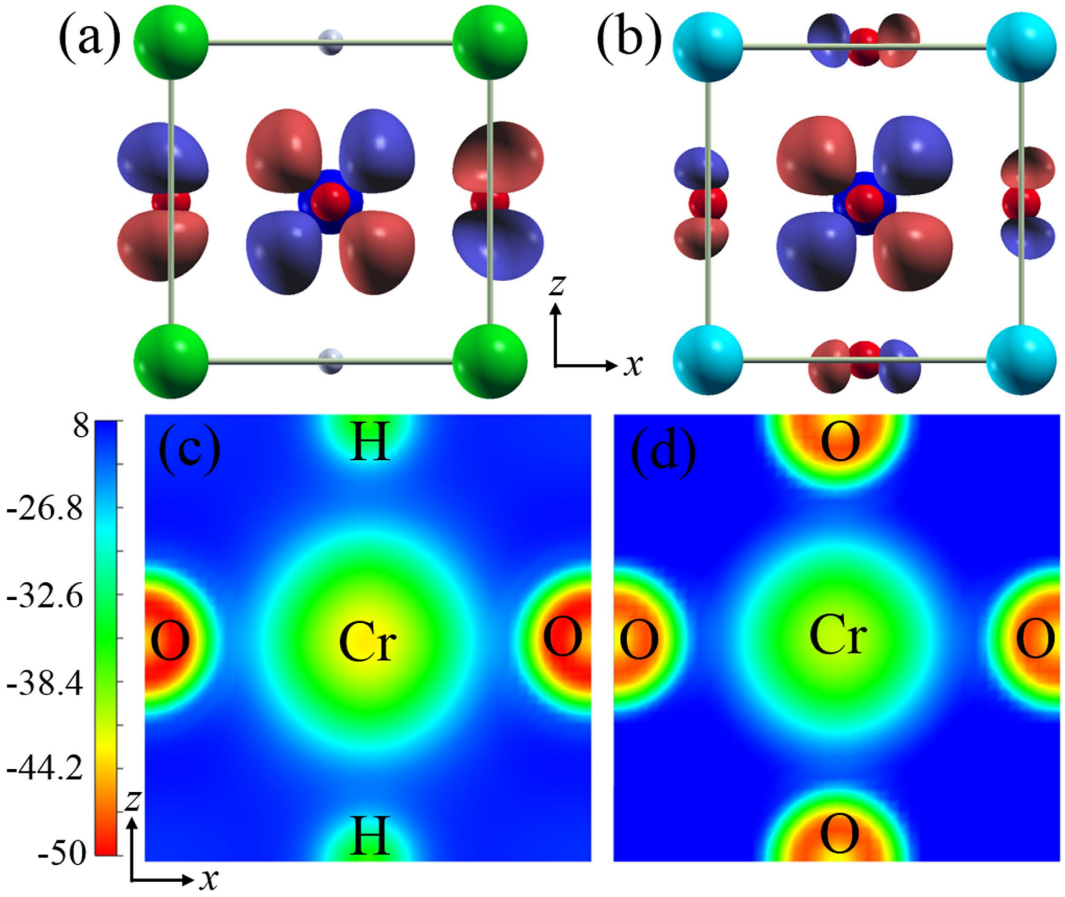

Figure 4. Isosurface plots of the Cr-d_{xz} like MLWFs for (a) cubic $SrCrO_2H$ and (b) cubic $LaCrO_3$. The lobes on the O^{2-} ion in the MLWF of $SrCrO_2H$ are bigger than those of $LaCrO_3$, indicating that the hybridization between Cr-d_{xz} orbital and O-p_z is stronger in $SrCrO_2H$. Contour plots of the electrostatic potential in (**c**) cubic $SrCrO_2H$ and (**d**) cubic $LaCrO_3$, projected on the *xz*-plane passing through Cr, H, and O sites. The electrostatic potential along the Cr-H direction is much weaker than that along the Cr-O direction in $SrCrO_2H$.

We propose that the stronger interaction between Cr-d_{xz} orbital and O-p_z orbital in $SrCrO_2H$ results from the more delocalized Cr-d_{xz} orbital in $SrCrO_2H$ (see Supplementary Figure S5). This is supported by a separate MLWF analysis which indicates that the spread of the atomic Cr-d_{xz} orbital in the cubic $SrCrO_2H$ is larger than that in the cubic $LaCrO_3$. The more delocalized Cr-d_{xz} orbital in $SrCrO_2H$ can be reasoned by considering the electrostatic potential exerted on the Cr 3*d* electrons. The contour plots of the electrostatic potential on the *x*-*z* plane are displayed in the Fig. 4c,d. We can see that the electrostatic potential along the Cr-H direction is much weaker than that along the Cr-O direction. Thus, the d_{xz} orbital in $SrCrO_2H$ is more delocalized along the *z*-axis, as can also be seen from Fig. 4a. It is the weaker repulsion between the H^- ion and the 3*d* electrons that makes the d_{xz} orbital in $SrCrO_2H$ more delocalized. The weaker electrostatic potential along the Cr-H direction results from the fact that H^- ions have the weaker electronegativity and less charge than O^{2-} ions. Therefore, the replacement of O^{2-} ions by H^- ions will not only change the hybridization type between the transition metal and the anions, but also affect the wavefunction distribution of *d* orbitals. Such novel mechanism revealed here for $SrCrO_2H$ can be also applied to $SrVO_2H$. The only difference is that there is one *d* electron less than that in $SrCrO_2H$, which makes the T_N slightly lower (see Supplementary Material). We note that first-principles calculations[34] were recently carried out to study the electronic and magnetic properties of $SrVO_2H$. However, the mechanism for the high Neel temperature in $SrVO_2H$ was not discovered.

The mechanism that the H^- ion induced delocalization of the *d* orbitals is general and may have profound effect on the electronic and magnetic properties of other perovskite oxyhydrides. Below we will predict that $SrFeO_2H$ has an extremely high T_N. With the cluster expansion approach, we predict that $SrFeO_2H$ takes the same ground state structure as that of $SrCrO_2H$. This is reasonable since the ionic radius of the Fe^{3+} ion is close to that of the Cr^{3+} ion. The optimized lattice constants *a* and *c* for $SrFeO_2H$ are 3.997 Å and 3.645 Å, respectively. The computed phonon dispersion[26] (see Supplementary Figure S4) indicates that $SrFeO_2H$ is dynamically stable. The spin exchange parameters calculated for the optimized $SrFeO_2H$ structures are listed in Table 1. $SrFeO_2H$ takes the G-type AFM order as the magnetic ground state since the NN AFM spin exchanges J_O (Fe-O-Fe) and J_H (Fe-H-Fe) are dominant. To our surprise, the spin exchange J_H (89.26 meV) in $SrFeO_2H$ is much stronger than J_O (39.63 meV) in $SrFeO_2H$. Note that the much stronger Fe-H-Fe interaction is not mainly caused by the shorter Fe-H distance than the Fe-O distance, because similar results are also obtained in the cubic perovskite $SrFeO_2H$

structure. In fact, the much stronger Fe-H-Fe interaction is mainly because the out-of-plane Fe-$d_{3z^2-r^2}$ orbital is more delocalized than the in-plane Fe-$d_{3x^2-r^2}$ and $d_{3y^2-r^2}$ orbitals. Therefore, the σ bond between the H 1*s* orbital and Fe-$d_{3z^2-r^2}$ orbital is much stronger than the σ bond between the O-2*p* orbitals and the in-plane Fe $d_{3x^2-r^2}/d_{3y^2-r^2}$ orbitals (see Supplementary Figure S6). Similar to the cases of $SrCrO_2H$ and $SrVO_2H$, the weaker electrostatic potential of H^- ions exerting on the *d* electrons of Fe^{3+} ions leads to more delocalized Fe-$d_{3z^2-r^2}$ orbitals, which results in an anomalously strong spin exchange J_H. Our MC simulations indicate that the T_N of $SrFeO_2H$ is around 826 K, which is even higher than that of $BiFeO_3$ ($T_N = 643$ K)[35] and $SrFeO_2$ with a quasi-two-dimensional structure ($T_N = 473$ K)[36,37]. Our result suggests that the replacement of O^{2-} ions by H^- ions can enhance the magnetic interactions not only in t_{2g} d^2 and d^3 systems, but also in d^5 systems. Our work suggests that the high magnetic transition temperature in $LaSrCoO_3H_{0.7}$[18–20] and $Sr_3Co_2O_{4.33}H_{0.84}$[21] should be also due to the H^- ion induced delocalization of the 3*d* e_g orbitals.

In summary, we perform a systematic theoretical study on the magnetic properties of perovskite oxyhydrides. The high magnetic transition temperature in $SrCrO_2H$ is revealed to be due to the delocalization of 3*d* orbitals in perovskite oxyhydrides. This is because H^- ions have weaker electronegativity and fewer electrons than O^{2-} ions. The more delocalized 3*d* orbitals in $SrCrO_2H$ make Cr-O-Cr superexchange strong and T_N high. This novel mechanism also applies to the case of $SrVO_2H$. We predict that the σ-type Fe-H-Fe interactions in $SrFeO_2H$ are extraordinarily strong which also result from the delocalization of the 3*d* orbitals. The delocalization of *d* orbitals in oxyhydrides discovered in this work is universal and may also have profound effects on properties other than the magnetic properties.

Methods

Our DFT calculations are performed on the basis of the projector augmented wave method[38,39] encoded in the Vienna ab initio simulation package[40,41] (VASP) using the generalized-gradient approximation (GGA) of Perdew, Burke, and Ernzerhof[42]. The plane-wave cutoff energy is set to be 450 eV. To properly describe the strong electron correlation in the 3*d* transition-metal oxide, the GGA plus on-site repulsion *U* method (GGA + *U*) is employed[43]. $U = 4$ eV and $J = 1$eV are applied to the 3*d* electron of Cr^{3+} ions. The maximally localized Wannier functions (MLWFs) are constructed with the Wannier90 program[44,45]. The spread functional is considered to be converged if the corresponding fractional change because two successive iterations is smaller than 10^{-10}. To find the ground state structures of $SrCrO_2H$, $SrVO_2H$, and $SrFeO_2H$, we adopt the cluster expansion approach[46] by using the alloy theoretic automation toolkit (ATAT)[47].

We perform parallel tempering Monte Carlo (PTMC) simulations[48,49] to estimate the magnetic transition temperature. In PTMC simulations, many replicas with different temperature are simultaneously simulated and a virtual process exchanging configuration of these replicas is introduced. PTMC simulations can avoid a local minimum at low temperatures and can reduce relaxation time. We adopt a $10 \times 10 \times 10$ supercell to perform PTMC simulations. Our test shows that the results obtained with a $12 \times 12 \times 12$ supercell are almost the same as those with the $10 \times 10 \times 10$ supercell. The number of replicas is set to 120.

References

1. Okuda, T., Nakanishi, K., Miyasaka, S. & Tokura, Y. Large Thermoelectric Response of Metallic Perovskites: $Sr_{1-x}La_xTiO_3$ ($0 \leq x \leq 0.1$). *Phys. Rev. B* **63,** 113104 (2001).
2. Dagotto, E., Hotta, T. & Moreo, A. Colossal Magnetoresistant Materials: The Key Role of Phase Separation. *Phys. Rep.* **344,** 1–153 (2001).
3. Moritomo, Y., Asamitsu, A., Kuwahara, H. & Tokura, Y. Giant Magnetoresistance of Manganese Oxides with a Layered Perovskite Structure. *Nature* **380,** 141–144 (1996).
4. Vonhelmolt, R., Wecker, J., Holzapfel, B., Schultz, L. & Samwer, K. Giant Negative Magnetoresistance in Perovskitelike $La_{2/3}Ba_{1/3}MnO_x$ Ferromagnetic Film. *Phys. Rev. Lett.* **71,** 2331–2333 (1993).
5. Bednorz, J. G. & Muller, K. A. Possible High T_c Superconductivity in the Ba-La-Cu-O System. *Z. Phys. B: Condens. Matter* **64,** 189–193 (1986).
6. Cohen, R. E. Origin of Ferroelectricity in Perovskite Oxides. *Nature* **358,** 136–138 (1992).
7. Johnston, D. C., Prakash, H., Zachariasen, W. H. & Viswanathan, R. High Temperature Superconductivity in the Li-Ti-O Ternary System. *Mater. Res. Bull.* **8,** 777–784 (1973).
8. Jansen, M. & Letschert, H. P. Inorganic Yellow-Red Pigments without Toxic Metals. *Nature* **404,** 980–982 (2000).
9. Kasahara, A. *et al.* Photoreactions on $LaTiO_2N$ under Visible Light Irradiation. *J. Phys. Chem. A* **106,** 6750–6753 (2002).
10. Zhang, Y. R., Masubuchi, Y., Motohashi, T., Kikkawa, S. & Hirota, K. Hot Isostatic Press Sintering and Dielectric Properties of $SrTaO_2N$ Ceramics. *Ceram. Int.* **39,** 3377–3380 (2013).
11. Zhang, Y.-R., Motohashi, T., Masubuchi, Y. & Kikkawa, S. Sintering and Dielectric Properties of Perovskite $SrTaO_2N$ Ceramics. *J. Eur. Ceram. Soc.* **32,** 1269–1274 (2012).
12. Tong, W., Yoon, W. S., Hagh, N. M. & Amatucci, G. G. A Novel Silver Molybdenum Oxyfluoride Perovskite as a Cathode Material for Lithium Batteries. *Chem. Mater.* **21,** 2139–2148 (2009).
13. Kobayashi, Y. *et al.* An Oxyhydride of $BaTiO_3$ Exhibiting Hydride Exchange and Electronic Conductivity. *Nat. Mater.* **11,** 507–511 (2012).
14. Sakaguchi, T. *et al.* Oxyhydrides of (Ca,Sr,Ba)TiO_3 Perovskite Solid Solutions. *Inorg. Chem.* **51,** 11371–11376 (2012).
15. Yajima, T. *et al.* Epitaxial Thin Films of $ATiO_{3-x}H_x$ (A = Ba, Sr, Ca) with Metallic Conductivity. *J. Am. Chem. Soc.* **134,** 8782–8785 (2012).
16. Bang, J. *et al.* Hydrogen Ordering and New Polymorph of Layered Perovskite Oxyhydrides: $Sr_2VO_{4-x}H_x$. *J. Am. Chem. Soc.* **136,** 7221–7224 (2014).
17. Yamamoto, T. *et al.* An Antiferro-to-Ferromagnetic Transition in $EuTiO_{3-x}H_x$ Induced by Hydride Substitution. *Inorg. Chem.* **54,** 1501–1507 (2015).
18. Blundell, S. J. *et al.* Magnetism in Oxide Chains Bridged with the Hydride Anion: $LaSrCoO_3H_{0.7}$ Studied Using Muon-Spin Rotation. *Physica B* **326,** 527–531 (2003).
19. Bridges, C. A., Darling, G. R., Hayward, M. A. & Rosseinsky, M. J. Electronic Structure, Magnetic Ordering, and Formation Pathway of the Transition Metal Oxide Hydride $LaSrCoO_3H_{0.7}$. *J. Am. Chem. Soc.* **127,** 5996–6011 (2005).
20. Hayward, M. A. *et al.* The Hydride Anion in an Extended Transition Metal Oxide Array: $LaSrCoO_3H_{0.7}$. *Science* **295,** 1882–1884 (2002).

21. Helps, R. M., Rees, N. H. & Hayward, M. A. $Sr_3Co_2O_{4.33}H_{0.84}$: an Extended Transition Metal Oxide-Hydride. *Inorg. Chem.* **49,** 11062–11068 (2010).
22. Tassel, C. *et al.* Direct Synthesis of Chromium Perovskite Oxyhydride with a High Magnetic-Transition Temperature. *Angew. Chem. Int. Ed.* **53,** 10377–10380 (2014).
23. Romero, F. D. *et al.* Strontium Vanadium Oxide-Hydrides: "Square-Planar" Two-Electron Phases. *Angew. Chem. Int. Ed.* **53,** 7556–7559 (2014).
24. Aleonard, R., Pauthene, R., Rebouill, J. P. & Veyret, C. Interpretation of the Magnetic Properties of the Rare Earth Chromites and the Rare Earth Manganites, *J. Appl. Phys.* **39,** 379 (1968).
25. Weinberg, I. & Larssen, P. Electron Paramagnetic Resonance and Antiferromagnetism in $LaCrO_3$. *Nature* **192,** 445–446 (1961).
26. Togo, A., Oba, F. & Tanaka, I. First-Principles calculations of the ferroelastic transition between rutile-type and $CaCl_2$-type SiO_2 at high pressures. *Phys. Rev. B* **78,** 134106 (2008).
27. Xiang, H. J., Kan, E. J., Wei, S.-H., Whangbo, M. H. & Gong, X. G. Predicting the Spin-Lattice Order of Frustrated Systems from First Principles. *Phys. Rev. B* **84,** 224429 (2011).
28. Xiang, H., Lee, C., Koo, H. J., Gong, X. & Whangbo, M. H. Magnetic Properties and Energy-Mapping Analysis. *Dalton. Trans.* **42,** 823–853 (2013).
29. Mitchell, R. H. & Chakhmouradian, A. R. A New Series of Complex Perovskites $La_{1-x}Sr_xCr_{1-x}Ti_xO_3$: Structural Characterization. *J. Solid State Chem.* **144,** 81–85 (1999).
30. Goodenough, J. B., Wickham, D. G. & Croft, W. J. Some Magnetic and Crystallographic Properties of the System $Li^+_xNi^{++}_{1-2x}Ni^{+++}_xO$. *J. Phys. Chem. Solids* **5,** 107–116 (1958).
31. Kanamori, J. Theory of the Magnetic Properties of Ferrous and Cobaltous Oxides, I. *Prog. Theor. Phys.* **17,** 177–196 (1957).
32. Kanamori, J. Theory of the Magnetic Properties of Ferrous and Cobaltous Oxides, II. *Prog. Theor. Phys.* **17,** 197–222 (1957).
33. Anderson, P. W. Antiferromagnetism - Theory of Superexchange Interaction. *Phys. Rev.* **79,** 350–356 (1950).
34. Wei, Y. *et al.* The Effect of Hydrogen Ordering on the Electronic and Magnetic Properties of the Strontium Vanadium Oxyhydride. *J. Phys. Condens. Matter*. **27,** 206001 (2015).
35. Wang, J. *et al.* Epitaxial $BiFeO_3$ Multiferroic Thin Film Heterostructures. *Science* **299,** 1719–1722 (2003).
36. Tsujimoto, Y. *et al.* Infinite-layer iron oxide with a square-planar coordination. *Nature* **450,** 1062–1065 (2007).
37. Xiang, H. J., Wei, S.-H. & Whangbo, M. H. Origin of the Structural and Magnetic Anomalies of the Layered Compound $SrFeO_2$: A Density Functional Investigation. *Phys. Rev. Lett.* **100,** 167207 (2008).
38. Blöchl, P. E. Projector augmented-wave method, *Phys. Rev. B* **50,** 17953–17979 (1994).
39. Kresse, G. & Joubert, D. From Ultrasoft Pseudopotentials to the Projector Augmented-Wave Method. *Phys. Rev. B* **59,** 1758–1775 (1999).
40. Kresse, G. & Furthmuller, J. Efficiency of ab-initio Total Energy Calculations for Metals and Semiconductors Using a Plane-Wave Basis Set. *Comp. Mater. Sci.* **6,** 15–50 (1996).
41. Kresse, G. & Furthmuller, J. Efficient Iterative Schemes for ab initio Total-Energy Calculations Using a Plane-Wave Basis Set. *Phys. Rev. B* **54,** 11169–11186 (1996).
42. Perdew, J. P., Burke, K. & Ernzerhof, M. Generalized Gradient Approximation Made Simple. *Phys. Rev. Lett.* **77,** 3865–3868 (1996).
43. Dudarev, S. L., Botton, G. A., Savrasov, S. Y., Humphreys, C. J. & Sutton, A. P. Electron-Energy-Loss Spectra and the Structural Stability of Nickel Oxide: An LSDA + *U* Study. *Phys. Rev. B* **57,** 1505–1509 (1998).
44. Mostofi, A. A. *et al.* wannier90: A Tool for Obtaining Maximally-Localised Wannier functions. *Comput. Phys. Commun.* **178,** 685–699 (2008).
45. Marzari, N., Mostofi, A. A., Yates, J. R., Souza, I. & Vanderbilt, D. Maximally Localized Wannier Functions: Theory and Applications. *Rev. Mod. Phys.* **84,** 1419–1475 (2012).
46. Ferreira, L. G., Wei, S. H. & Zunger, A. First-principles Calculation of Alloy Phase Diagrams: The Renormalized-Interaction Approach. *Phys. Rev. B* **40,** 3197–3231 (1989).
47. van de Walle, A., Asta, M. & Ceder, G. The Alloy Theoretic Automated Toolkit: A User Guide. *Calphad.* **26,** 539–553 (2002).
48. Hukushima, K. & Nemoto, K. Exchange Monte Carlo Method and Application to Spin Glass Simulations. *J. Phys. Soc. Jpn.* **65,** 1604–1608 (1996).
49. Wang, P. S., Ren, W., Bellaiche, L. & Xiang, H. J. Predicting a Ferrimagnetic Phase of Zn_2FeOsO_6 with Strong Magnetoelectric Coupling. *Phys. Rev. Lett.* **114,** 147204 (2015).

Acknowledgements

This work was supported by NSFC (11374056), the Special Funds for Major State Basic Research (2012CB921400, 2015CB921700), Program for Professor of Special Appointment (Eastern Scholar), Fok Ying Tung Education Foundation, FANEDD, and NCET-10-0351.

Additional Information

Supplementary information accompanies this paper at http://www.nature.com/srep

Competing financial interests: The authors declare no competing financial interests.

How to cite this article: Liu, K. *et al.* Orbital Delocalization and Enhancement of Magnetic Interactions in Perovskite Oxyhydrides. *Sci. Rep.* **6**, 19653; doi: 10.1038/srep19653 (2016).